



## miR-101 suppresses the development of MLL-rearranged acute myeloid leukemia

by Estrella Gonzales-Aloy, Patrick Connerty, Basit Salik, Bing Liu, Andrew J. Woo, Michelle Haber, Murray D. Norris, Jianlong Wang, and Jenny Y. Wang

Haematologica 2019 [Epub ahead of print]

*Citation: Estrella Gonzales-Aloy, Patrick Connerty, Basit Salik, Bing Liu, Andrew J. Woo, Michelle Haber, Murray D. Norris, Jianlong Wang, and Jenny Y. Wang. miR-101 suppresses the development of MLL-rearranged acute myeloid leukemia.*

*Haematologica. 2019; 104:xxx*

*doi:10.3324/haematol.2018.209437*

### *Publisher's Disclaimer.*

*E-publishing ahead of print is increasingly important for the rapid dissemination of science. Haematologica is, therefore, E-publishing PDF files of an early version of manuscripts that have completed a regular peer review and have been accepted for publication. E-publishing of this PDF file has been approved by the authors. After having E-published Ahead of Print, manuscripts will then undergo technical and English editing, typesetting, proof correction and be presented for the authors' final approval; the final version of the manuscript will then appear in print on a regular issue of the journal. All legal disclaimers that apply to the journal also pertain to this production process.*

## **miR-101 suppresses the development of *MLL*-rearranged acute myeloid leukemia**

Estrella Gonzales-Aloy,<sup>1</sup> Patrick Connerty,<sup>1</sup> Basit Salik,<sup>1</sup> Bing Liu,<sup>2</sup> Andrew J. Woo,<sup>3</sup> Michelle Haber,<sup>4</sup> Murray D. Norris,<sup>4</sup> Jianlong Wang<sup>5</sup> and Jenny Y. Wang<sup>1\*</sup>

<sup>1</sup>Cancer and Stem Cell Biology Group, Children's Cancer Institute, University of New South Wales, Sydney, NSW 2052, Australia

<sup>2</sup>Kids Cancer Alliance, Translational Cancer Research Centre for Kids, Cancer Institute New South Wales, Sydney, NSW 2052, Australia

<sup>3</sup>Harry Perkins Institute of Medical Research, QEII Medical Centre, Nedlands and Centre for Medical Research, The University of Western Australia, Crawley, WA 6009, Australia

<sup>4</sup>Children's Cancer Institute, University of New South Wales, Sydney, NSW 2052, Australia

<sup>5</sup>Department of Cell, Developmental and Regenerative Biology, Black Family Stem Cell Institute, Icahn School of Medicine at Mount Sinai, New York, NY10029

**Running title:** miR-101 as a novel tumor suppressor in AML

**\*Corresponding author:** Jenny Y. Wang, [jwang@ccia.unsw.edu.au](mailto:jwang@ccia.unsw.edu.au).

Dysregulation of miRNAs (a class of short noncoding RNAs) has been observed in solid tumors and leukemia,<sup>1,2</sup> and the role of miRNAs in cancer development is largely context-dependent.<sup>2</sup> While several miRNAs (e.g., miR-29b)<sup>3</sup> have been functionally linked to acute myeloid leukemia (AML), their antitumor effects *in vivo* are not evident, possibly due to the complexity and diversity of miRNA-mediated gene regulation. It remains unclear how miRNAs contribute to an aggressive phenotype in heterogeneous AML. Using an integrated miRNA and mRNA expression analysis, here we uncover a miRNA-regulatory network composed of eight miRNAs (i.e., miR-29a/b, miR-101, miR-222, miR-26b, miR-27b, miR-140 and miR-155) whose downregulation is associated with leukemia aggressiveness. We also define a tumor suppressive role for miR-101 in the development of *mixed-lineage leukemia (MLL)*-rearranged AML. Restoration of miR-101 expression significantly impedes leukemia initiation and progression through induction of cell cycle inhibitors and inhibition of genes associated with self-renewal and pro-survival in leukemic stem cells (LSCs).

Oncogenic rearrangement of the *MLL* gene in hematopoietic stem/progenitor cells (HSPCs) induces aberrant gene expression and confers a poor clinical prognosis in acute leukemias. Transformation by MLL fusion proteins is primarily mediated through direct upregulation of the *HOXA*-cluster genes and HOX cofactors such as MEIS1.<sup>4</sup> HOXA9 and MEIS1 are the most essential downstream effectors of MLL fusion proteins, and we have previously reported that their co-expression is sufficient to predispose HSPCs to malignant transformation and induce AML.<sup>5</sup> Aberrant overexpression of HOXA9 and MEIS1 is required for the induction and maintenance of *MLL*-rearranged AML, where LSCs have been functionally defined.<sup>4,5</sup>

We and others have shown that MLL fusion proteins (e.g., MLL-AF9) can serve as an initiating event for oncogenic conversion of normal HSPCs into pre-LSCs, which subsequently acquire additional events upon transplantation into mice for the development of LSCs.<sup>4,7</sup> The self-renewal

rate in a pre-leukemic clone determines subsequent tumorigenic potential *in vivo*. We have previously demonstrated that pre-LSCs transformed from normal HSPCs by MLL-AF9 have higher self-renewal potential and produce a more aggressive leukemia in mice with shorter latency than pre-LSCs transformed by HOXA9/MEIS1.<sup>5,7</sup> Despite major differences in self-renewal and mouse survival, pre-LSCs mediated by MLL-AF9 and HOXA9/MEIS1 display similar immunophenotype and induce AML with similar histopathologic manifestations.<sup>5,7</sup> Thus, genes differentially expressed in MLL-AF9 versus HOXA9/MEIS1 pre-LSCs may contribute to the highly aggressive phenotype in MLL-AF9-induced AML.

To identify miRNAs that regulate the differential gene expression, we performed an integrated analysis for miRNA and mRNA expression profiling using the Bayesian Network with Splitting-Averaging strategy,<sup>8</sup> and identified a tumor suppressive miRNA-regulatory network in HSPC-derived MLL-AF9 versus HOXA9/MEIS1 pre-LSCs<sup>4,7</sup> (**Figure 1A; Supplementary Figure S1A-D**). Of the eight miRNAs identified, miR-101, miR-29b, miR-222 and miR-155 are reportedly downregulated in newly-diagnosed AML patient samples compared to normal human CD34<sup>+</sup> HSPCs, while miR-29a and miR-29b are downregulated in patients with *MLL*-rearranged AML compared to other AML subtypes displaying a subtype-specific feature.<sup>9</sup> These observations are consistent with our result showing lower levels of these miRNAs in LSCs (L-GMP, Lin<sup>-</sup>CD127<sup>-</sup>c-Kit<sup>+</sup>Sca1<sup>-</sup>GFP<sup>+</sup>CD16/32<sup>high</sup>CD34<sup>+</sup>)<sup>4</sup> flow-sorted from mice with MLL-AF9-induced AML than in normal murine HSPCs (**Supplementary Figure S1E**), supporting a potential tumor suppressor role for the miRNA-regulatory network in *MLL*-rearranged AML.

Among the eight miRNAs, miR-29b has been functionally defined as a tumor suppressor and its overexpression reduced tumorigenicity in a BCR-ABL-expressed K562 xenograft mouse model of human chronic myeloid leukemia (CML) by targeting apoptosis, cell cycle and proliferation pathways.<sup>3</sup> While miR-101 is reported as a putative tumor suppressor in several types of cancer via

targeting diverse oncogenic pathways,<sup>10</sup> its role in AML has not yet been explored. To further evaluate the miRNA-regulatory network, we investigated the tumor suppressive function of miR-101, which was one of the most downregulated miRNAs identified, in MLL-AF9-induced AML. We used miR-150 as a control because, despite not being in the network, its expression is downregulated in both AML and CML.<sup>11</sup>

HSPC-derived MLL-AF9 pre-LSCs were transduced with a retroviral vector expressing miR-101, miR-29b or miR-150. Ectopic expression of these miRNAs reduced the ability of pre-LSCs to form colonies in serial replating assays (**Figure 1B; Supplementary Figure S2A-B**). Notably, miR-101 induced a significantly stronger growth-inhibitory effect on MLL-AF9 pre-LSCs than miR-29b and miR-150, which was correlated with miR-101-mediated upregulation of cell-cycle inhibitor *p21/Cdkn1a* and downregulation of key Wnt/self-renewal target genes, including *Meis1*, *c-Fos*, *Mef2c*, *Bcl11a*, *CD52*, *Gpx3* and *Ly6e* identified by microarray analysis (**Figure 1C**). Subsequent RT-PCR and western blot analyses confirmed increased expression of p21 and reduced levels of Meis1, Bcl11a, c-Fos and Tcf7l2, which are known self-renewal genes in MLL-AF9-induced AML<sup>4,5,7</sup> (**Figure 1D; Supplementary Figure S2C**). We and others have previously demonstrated that Wnt/ $\beta$ -catenin signaling is required for the development of LSCs in AML.<sup>5</sup> Tcf7l2 and c-Fos are two key  $\beta$ -catenin transcriptional cofactors driving transcription of Wnt/ $\beta$ -catenin target genes likely contributing to LSC self-renewal.<sup>7</sup> Furthermore, the phenotypic defect in pre-LSCs was accompanied by decreased cell proliferation in methylcellulose and induced apoptotic cell death through suppression of pro-survival proteins Mcl-1 and Bcl-2, as well as G1 cell cycle arrest through elevation of cell-cycle inhibitors p21 and p27 (**Figure 1E-F; Supplementary Figure S2D**). These findings suggest that restoring expression of miR-101 impairs pre-LSC functions through regulation of genes associated with Wnt/self-renewal, pro-survival and cell cycle pathways.

We next assessed the inhibitory effect of miR-101 overexpression on AML development by intravenously transplanting miR-101-expressing MLL-AF9 pre-LSCs into sublethally irradiated syngeneic recipient mice. Our data showed that enforced expression of miR-101 reduced the incidence and delayed the onset and progression of AML in mice, which was accompanied by a significant decrease in leukemic cell infiltration in bone marrow (BM, **Figure 2A-B**). miR-101-expressing MLL-AF9 LSCs flow-sorted from primary AML revealed reduced colony-forming capacity (**Figure 2C; Supplementary Figure S3**). This was likely caused by miR-101-induced suppression of Wnt target genes (*Tcf7l2* and *c-Fos*), and cell cycle arrest at the G1 phase via upregulation of p21, p27 and Gadd45a (**Figure 2D**). As a consequence of compromised LSCs, miR-101-expressing AML cells from primary recipients generated a less aggressive leukemia in secondary recipient mice, whose BM cells exhibited a marked decrease in nuclear active  $\beta$ -catenin (**Figure 2E**). Altogether, these data underscore a tumor suppressor role for miR-101, whose ectopic expression impairs LSC development and reduces AML aggressiveness in mice.

We then investigated the effect of miR-101 overexpression on tumor burden in a mouse xenograft model of human MLL-AF9 (MOLM-13) AML, which has an extremely short latency (14 days) and is an effective xenotransplantation model for *in vivo* functional studies. Consistent with our observation in murine MLL-AF9 leukemic cells, stable overexpression of miR-101 substantially decreased nuclear active  $\beta$ -catenin in MOLM-13 cells (**Figure 3A; Supplementary Figure S4A**). *In vivo* bioluminescence imaging showed that miR-101 overexpression reduced engraftment of human MOLM-13 leukemic cells in NOD/SCID/IL2R gamma-null (NSG) mice without affecting bone marrow homing (**Figure 3B-C; Supplementary Figure S4B**).

In agreement with miR-101-induced inhibition of leukemia cell proliferation *in vivo*, miR-101 markedly decreased the expression and phosphorylation of c-FOS (**Figure 3D**), a known  $\beta$ -catenin transcriptional cofactor implicated in the regulation of cell growth, survival, apoptosis,

transformation and oncogenesis.<sup>12</sup> Phosphorylation of c-FOS is essential for its protein stabilization and maximal transactivation contributing to its increased cell-transforming activity.<sup>13</sup> *c-FOS* is reportedly a direct target of several miRNAs, including miR-101, miR-29 and miR-222.<sup>14</sup> Our data confirmed a miR-101-mediated reduction in luciferase activity from the construct containing the *c-FOS* 3'-UTR (**Supplementary Figure S4C**). Enforced expression of exogenous c-FOS prevented miR-101-induced inhibition of leukemic cell viability (**Supplementary Figure S4D-E**). This result supports the role for c-FOS as a functional downstream target of miR-101.

Notably, restoration of miR-101 upregulated the miRNA co-expression network, including miR-26b, miR-27b, miR-29a, miR-140 and miR-222, but did not alter the expression of miR-150 (**Figure 3E**). miR-101 is reportedly a direct regulator of histone methyltransferase EZH2 and likely regulates the miRNA network through modulation of EZH2-mediated H3K27me3. EZH2 augments MLL-AF9-initiated leukemogenesis by enhancing a myeloid differentiation block in AML.<sup>15</sup> Our data showed that overexpression of miR-101 reduced levels of EZH2 and H3K27me3 in murine MLL-AF9 pre-LSCs and human MLL-AF9 (MOLM-13) AML cells (**Supplementary Figure S5A**). Selective inhibition of EZH2 by EZH2 inhibitor EPZ-6438 caused a marked increase in miR-26b, miR-27b, miR-29b and miR-140 without affecting miR-150 (**Supplementary Figure S5B**), underlining epigenetic regulation of the miRNA network. Interestingly, we also observed EZH2 inhibitor-induced elevation of miR-101 (**Supplementary Figure S5B**). It is likely that there is a mutual regulation between miR-101 and EZH2-mediated H3K27me3. Increased miR-101 suppresses H3K27me3 by directly targeting EZH2; conversely, reduced H3K27me3 restores expression of the miRNA network including miR-101. These findings collectively suggest that miR-101 exerts its gene regulatory function in leukemogenesis, at least in part, by activating and cooperating with the network components. This cooperation between the miRNAs allows for the simultaneous targeting of multiple oncogenic pathways that maximizes the tumor suppressive effect of miR-101.

In conclusion, we report here a miRNA-regulatory network associated with disease aggressiveness and demonstrate a tumor suppressor role for miR-101 in *MLL*-rearranged AML. Enforced expression of miR-101 impairs LSC self-renewal and restrains leukemia development in mice. Together with prior findings showing a tumor suppressor role for miR-29b in leukemia,<sup>3</sup> our data support the value of the miRNA co-expression network as potential novel targets for miRNA-based therapies in AML.

**Acknowledgements:** We thank the staff of the Mark Wainwright Analytical Centre for their technical assistance. J.Y.W. was supported by NHMRC APP1128824 and Tour de Cure Senior Research Grant 17-UNSW-RS-03.

## References

1. Lu J, Getz G, Miska EA, et al. MicroRNA expression profiles classify human cancers. *Nature*. 2005;435(7043):834-838.
2. Calin GA, Croce CM. MicroRNA signatures in human cancers. *Nat Rev Cancer*. 2006;6(11):857-866.
3. Garzon R, Heaphy CE, Havelange V, et al. MicroRNA 29b functions in acute myeloid leukemia. *Blood*. 2009;114(26):5331-5341.
4. Krivtsov AV, Twomey D, Feng Z, et al. Transformation from committed progenitor to leukaemia stem cell initiated by MLL-AF9. *Nature*. 2006;442(7104):818-822.
5. Wang Y, Krivtsov AV, Sinha AU, et al. The Wnt/beta-catenin pathway is required for the development of leukemia stem cells in AML. *Science*. 2010;327(5973):1650-1653.
6. Lynch JR, Yi H, Casolari DA, et al. Gαq signaling is required for the maintenance of MLL-AF9 induced AML. *Leukemia*. 2016;30(8):1745-1748.
7. Dietrich PA, Yang C, Leung HH, et al. GPR84 sustains aberrant beta-catenin signaling in leukemic stem cells for maintenance of MLL leukemogenesis. *Blood*. 2014;124(22):3284-3294.
8. Liu B, Li J, Tsykin A, et al. Exploring complex miRNA-mRNA interactions with Bayesian networks by splitting-averaging strategy. *BMC Bioinformatics*. 2009;10:408.
9. Garzon R, Volinia S, Liu CG, et al. MicroRNA signatures associated with cytogenetics and prognosis in acute myeloid leukemia. *Blood*. 2008;111(6):3183-3189.
10. Varambally S, Cao Q, Mani R-S, et al. Genomic Loss of microRNA-101 Leads to Overexpression of Histone Methyltransferase EZH2 in Cancer. *Science*. 2008;322(5908):1695-1699.
11. He Y, Jiang X, Chen J. The role of miR-150 in normal and malignant hematopoiesis. *Oncogene*. 2013;33(30):3887-3893.
12. Eferl R, Wagner EF. AP-1: a double-edged sword in tumorigenesis. *Nat Rev Cancer*. 2003;3(11):859-868.
13. Sasaki T, Kojima H, Kishimoto R, et al. Spatiotemporal regulation of c-Fos by ERK5 and the E3 ubiquitin ligase UBR1, and its biological role. *Mol Cell*. 2006;24(1):63-75.
14. Liu J-J, Lin X-J, Yang X-J, et al. A novel AP-1/miR-101 regulatory feedback loop and its implication in the migration and invasion of hepatoma cells. *Nucleic Acids Res*. 2014;42(19):12041-12051.
15. Tanaka S, Miyagi S, Sashida G, et al. Ezh2 augments leukemogenicity by reinforcing differentiation blockage in acute myeloid leukemia. *Blood*. 2012;120(5):1107-1117.

## Figure legends

### Figure 1. Overexpression of miR-101 impairs the function of MLL-AF9 pre-LSCs.

(A) Integrated genomic analysis identifying a tumor suppressor miRNA-regulatory network in MLL-AF9 pre-LSCs compared to HOXA9/MEIS1 pre-LSCs. Diamond shape: miRNAs identified by Exiqon miRCURY LNA microRNA array. Circle: mRNA (targeted by miRNAs) identified by Illumina expression array. (B) Serial colony replating assay of miRNA-expressing MLL-AF9 pre-LSCs. The number of colonies per dish at the 6<sup>th</sup> round of replating is shown (n=3). (C) Heat map of microarray analysis showing differential gene expression in MLL-AF9 pre-LSCs overexpressing miR-101 versus empty vector (EV) control (n=3) with a cut-off of the false discovery rate (FDR)  $\leq 0.05$  and fold change (FC)  $\geq 1.5$ . (D) Western blotting confirming miR-101-induced downregulation of Meis1 and c-Fos expression in MLL-AF9 pre-LSCs. (E) Percentage of apoptotic cells (n=3) in MLL-AF9 pre-LSCs and western blotting showing reduced expression of Mcl-1 and Bcl-2 by miR-101 overexpression. (F) Cell cycle analysis of miR-101-expressing MLL-AF9 pre-LSCs using Ki-67 and 7AAD staining (n=3 independent experiments) and western blotting revealing miR-101-induced upregulation of p21 and p27 expression. \*,  $P < 0.05$ ; \*\*,  $P < 0.01$ ; NS, not significant ( $P > 0.05$ ).

**Figure 2. miR-101 suppresses the development of LSCs in a mouse model of MLL-AF9-driven AML.** (A) Kaplan-Meier survival curves of mice receiving miR-101-expressing MLL-AF9 pre-LSCs.  $1 \times 10^6$  pre-LSCs were transplanted into sublethally irradiated (6 Gy) BL6 recipient mice for the development of primary AML. *P* was determined by the log-rank test. (B) Percentages of GFP<sup>+</sup> leukemic cells in the BM of mice with primary AML. (C) Colony forming assay of MLL-AF9 LSCs from primary AML. (D) RT-qPCR analysis of *Tcf7l2* and *c-Fos* gene expression, cell cycle analysis and expression of p21, p27 and Gadd45a proteins in primary MLL-AF9 LSCs. (E) Kaplan-Meier survival curves of mice receiving GFP<sup>+</sup> MLL-AF9 leukemic cells isolated from primary AML and confocal immunofluorescence showing miR-101-induced reduction of nuclear active  $\beta$ -catenin in leukemic cells from secondary AML. \*, *P* < 0.05; \*\*\*, *P* < 0.0005, \*\*\*\*, *P* < 0.0001; NS, not significant (*P* > 0.05).

**Figure 3. miR-101 reduces tumor burden in human MLL-AF9 (MOLM-13) xenografts.**

(A) Confocal immunofluorescence confirming miR-101-induced decrease of nuclear active  $\beta$ -catenin in human MLL-AF9 (MOLM-13) AML cells. (B) Bioluminescence imaging and total flux (photons/sec; p/s) of MOLM-13 xenograft mice (n=4). (C) Percentage of hCD45<sup>+</sup> cells engrafted in the BM of MOLM-13 xenograft mice. (D) Western blot analysis showing miR-101-induced reduction in p-c-FOS<sup>Ser32</sup> and c-FOS levels. (E) RT-qPCR analysis of miRNA expression in miR-101-expressing human MLL-AF9 AML cells isolated from the BM of MOLM-13 xenograft mice. \*\*,  $P < 0.01$ ; \*\*\*,  $P < 0.0005$ ; \*\*\*\*,  $P < 0.0001$ ; NS, not significant ( $P > 0.05$ ).

**Figure 1**

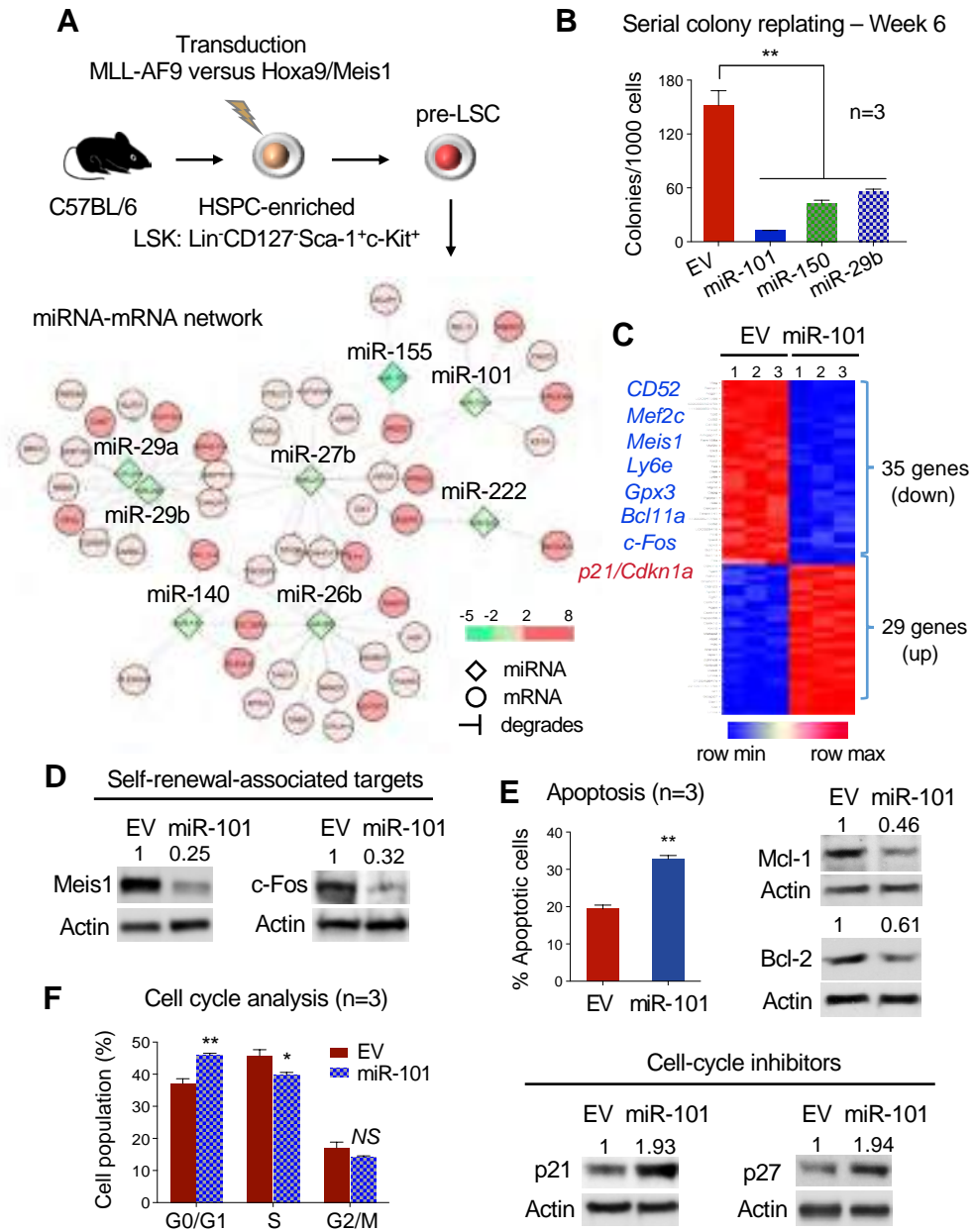


**Figure 2**

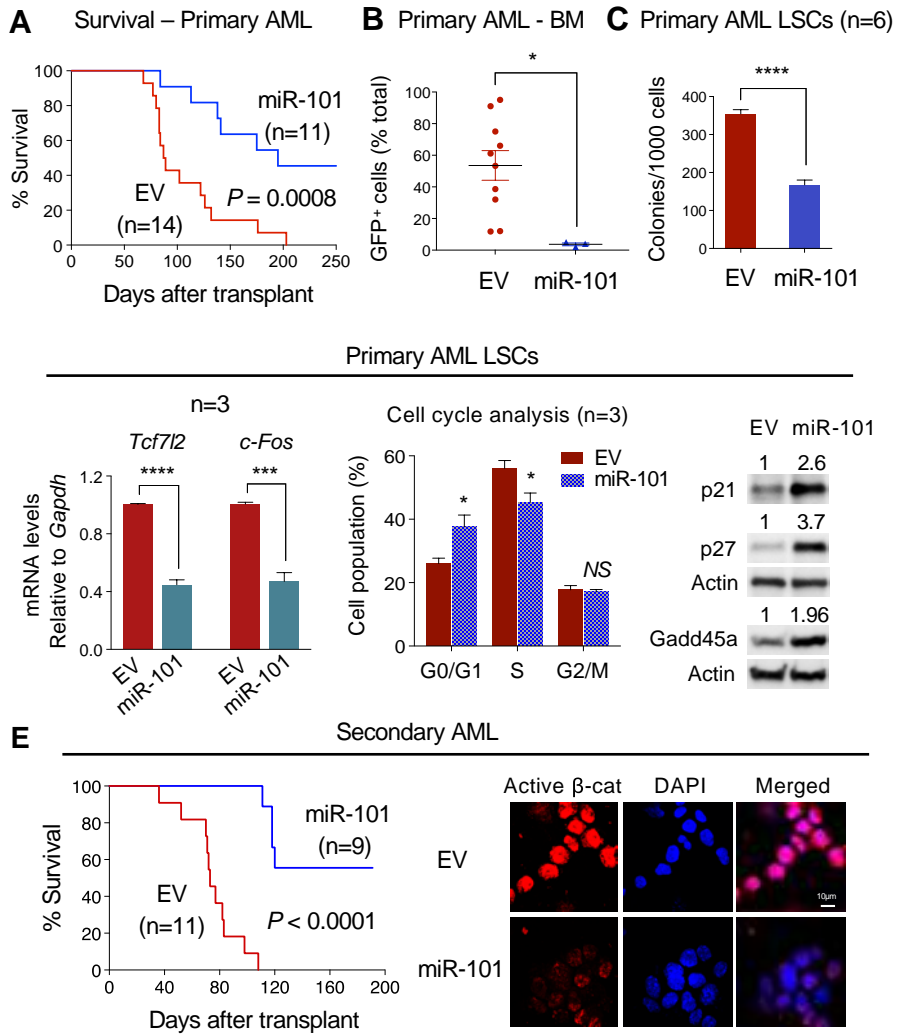
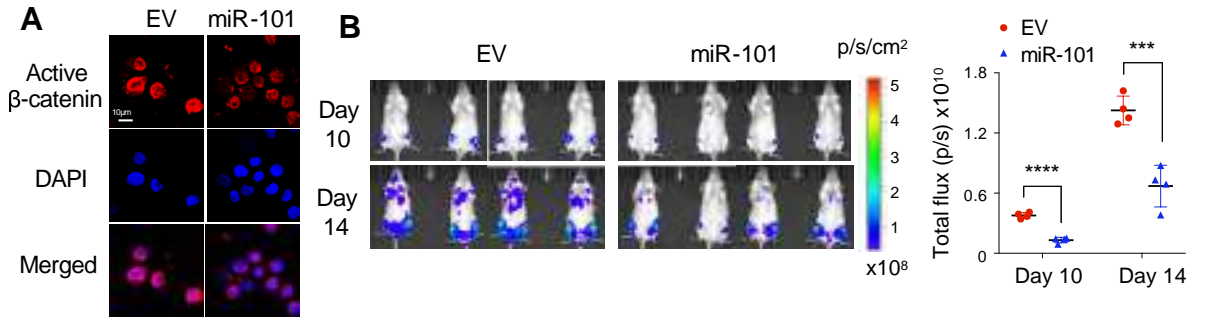
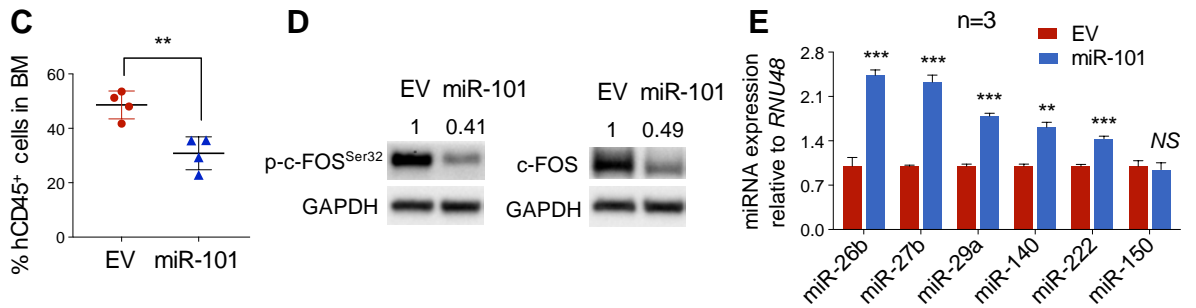


**Figure 3**

Human MLL-AF9 (MOLM-13) AML

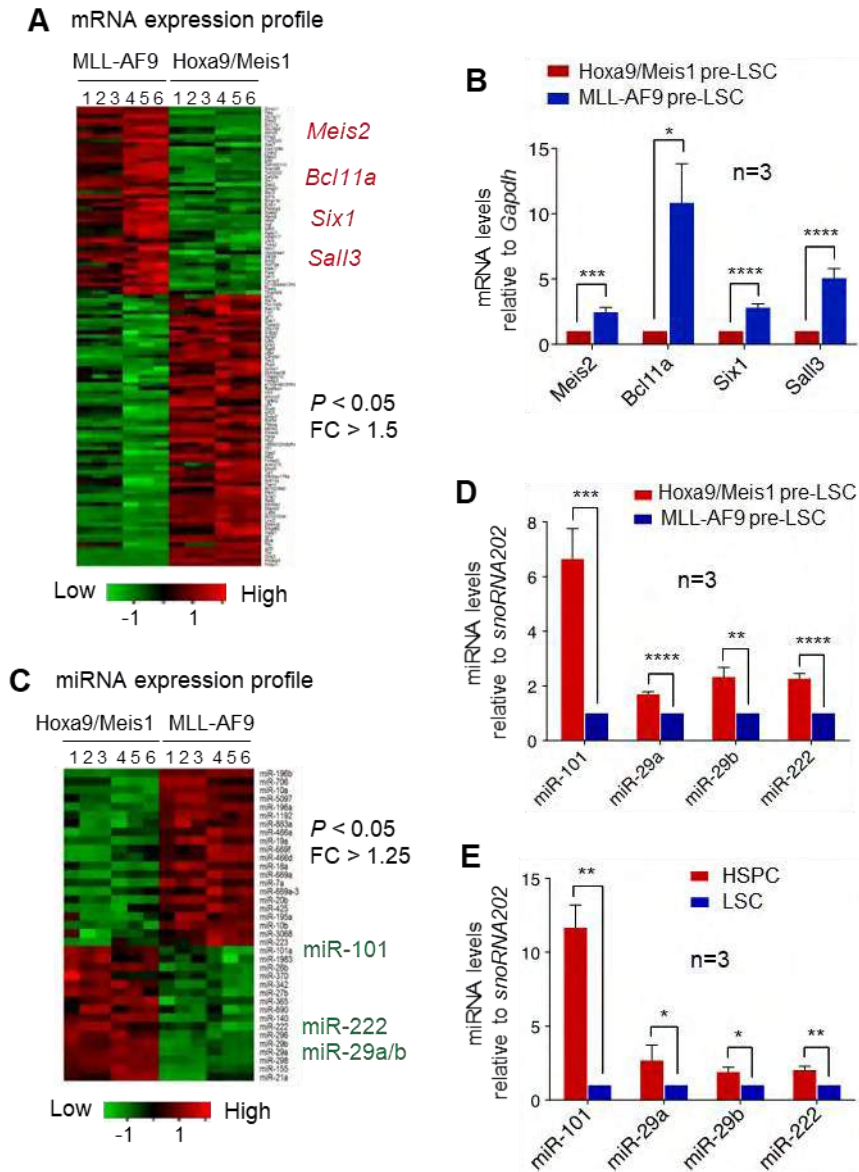


MOLM-13 xenograft - Day14 post-transplantation

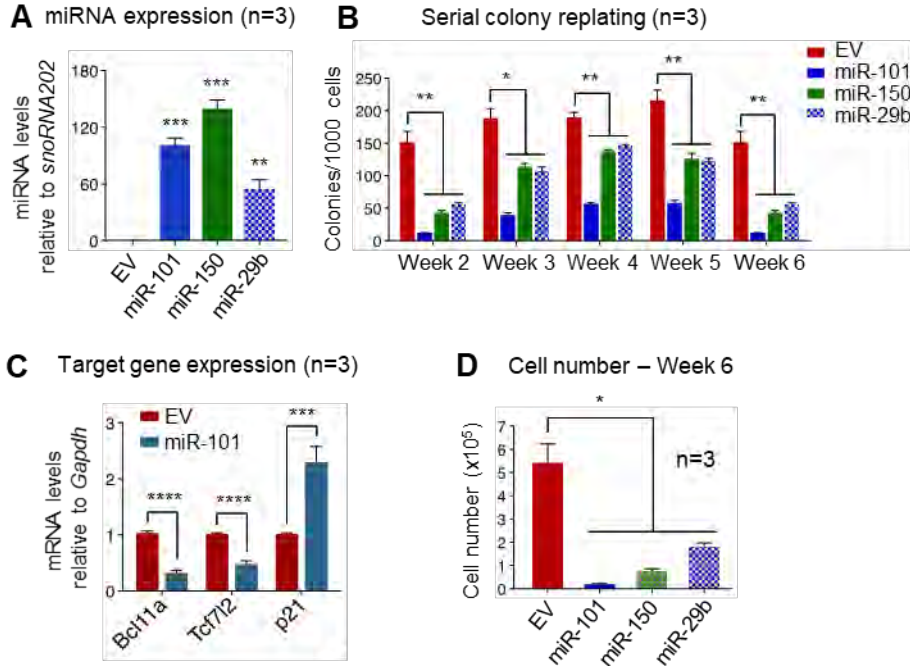


## Supplementary information

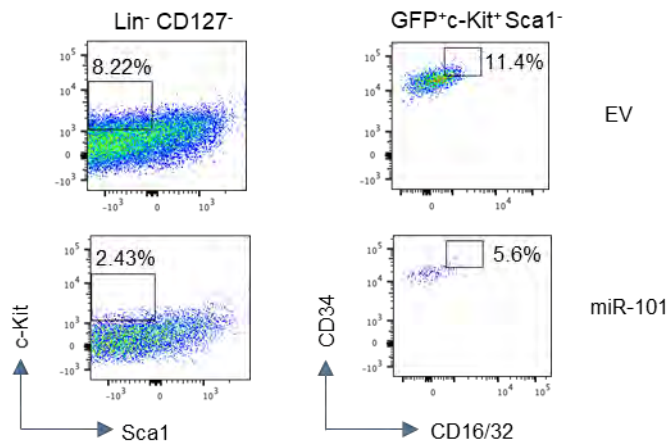
### miR-101 suppresses the development of *MLL*-rearranged acute myeloid leukemia



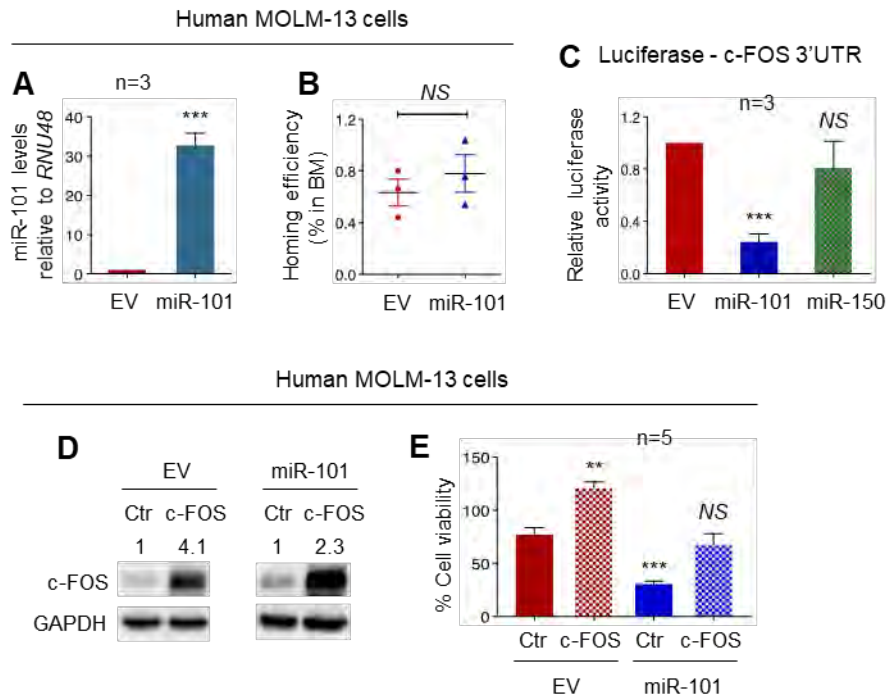
**Supplementary Figure 1.** (A) Heat map representation of microarray analysis showing differential gene expression in MLL-AF9 versus Hoxa9/Meis1 pre-LSCs ( $n=6$ ) with a cut-off of  $P < 0.05$  and  $FC > 1.5$ . (B) RT-qPCR analysis confirming differential expression of genes identified by microarray analysis in MLL-AF9 versus Hoxa9/Meis1 pre-LSCs. (C) Heat map representation of Exiqon miRCURY LNA microRNA array analysis showing differential miRNA expression in MLL-AF9 versus Hoxa9/Meis1 pre-LSCs ( $n=6$ ) with a cut-off of  $P < 0.05$  and  $FC > 1.25$ . (D and E) RT-qPCR analysis validating miRNA expression in MLL-AF9 versus Hoxa9/Meis1 pre-LSCs (D) and in MLL-AF9 LSCs versus normal HSPCs (E). Results were normalized using *snoRNA202* as control. Error bars are shown as mean  $\pm$  SEM of three independent experiments unless specified otherwise. \*,  $P < 0.05$ ; \*\*,  $P < 0.01$ ; \*\*\*,  $P < 0.0005$ ; \*\*\*\*,  $P < 0.0001$ .



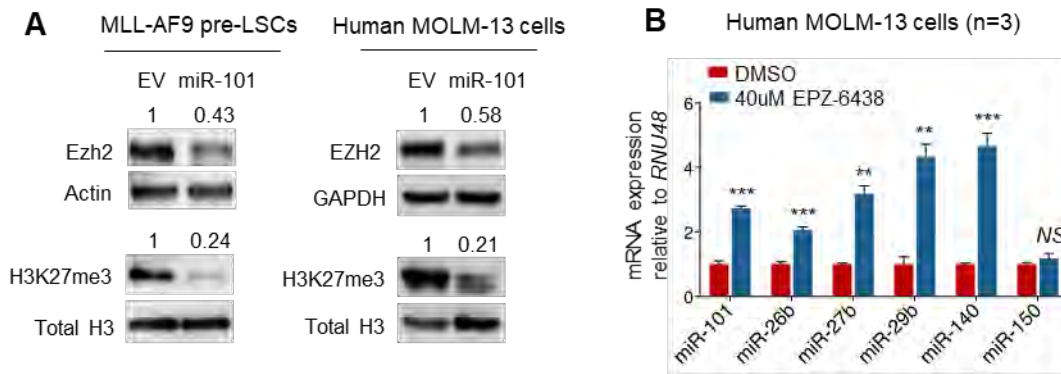
**Supplementary Figure 2.** (A) RT-qPCR analysis confirming miRNA overexpression in MLL-AF9 pre-LSCs transduced with miR-101, miR-150 and miR-29b, respectively. (B) Serial colony replating assay of miRNA-expressing MLL-AF9 pre-LSCs. *Note:* The number of colonies produced from week 1 is not shown given cells under selection in the first week post-transduction. (C) RT-qPCR confirming miR-101 target gene expression in MLL-AF9 pre-LSCs. (D) Total numbers of expanded MLL-AF9 pre-LSCs after a 5-day incubation in methylcellulose supplemented with appropriate cytokines. The cell number per dish at the 6<sup>th</sup> round of replating is shown (n=3). \*,  $P < 0.05$ ; \*\*,  $P < 0.01$ ; \*\*\*,  $P < 0.0005$ ; \*\*\*\*,  $P < 0.0001$ .



**Supplementary Figure 3.** Representative flow plots depicting changes in the LSC population ( $\text{Lin}^- \text{CD127}^- \text{c-Kit}^+ \text{Sca1}^- \text{GFP}^+ \text{CD16/32}^{\text{high}} \text{CD34}^+$ ) upon miR-101 overexpression in the BM of mice that developed primary MLL-AF9 AML.



**Supplementary Figure 4.** (A) RT-qPCR confirming miR-101 overexpression in transduced human MLL-AF9 (MOLM-13) cells. (B) BM homing of human MOLM-13 cells expressing EV versus miR-101, assessed 21 hours after transplantation.  $1 \times 10^6$  cells were transplanted into NSG mice (n=3) and human AML cells were identified from mouse BM by staining for human CD45 and FACS analysis. (C) Luciferase activity of the c-FOS 3'UTR reporter gene in the absence or presence of miR-101 and miR-150, respectively. miR-150 served as a control miRNA as it has no predicted binding sites in the 3'UTRs of *c-FOS*. HEK293T cells were cotransfected with the reporter constructs for luciferase assays. \*\*\*,  $P < 0.0005$ ; NS, not significant ( $P > 0.05$ ). (D) Western blot analysis confirming enforced overexpression of c-FOS in human MOLM-13 cells expressing EV or miR-101. (E) Relative changes in cell viability upon c-FOS overexpression in human MOLM-13 cells expressing EV versus miR-101. \*,  $P < 0.05$ ; \*\*,  $P < 0.01$ ; \*\*\*,  $P < 0.0005$ ; NS, not significant ( $P > 0.05$ ).



**Supplementary Figure 5.** (A) Western blot analysis showing miR-101-induced reduction in levels of EZH2 and H3K27me3 in murine MLL-AF9 pre-LSCs and human MLL-AF9 (MOLM-13) AML cells. (B) RT-qPCR analysis of miRNA expression alteration in response to a selective EZH2 inhibitor, EPZ-6438, in human MOLM-13 cells. \*\*,  $P < 0.01$ ; \*\*\*,  $P < 0.0005$ ; NS, not significant ( $P > 0.05$ ).

## Methods

### Mice

Six- to 8-week-old C57BL/6 (BL6) and NSG female mice were obtained from Australian BioResources, Mossvale, NSW, Australia. All animal experiments were approved by the Animal Ethics Committee of the University of New South Wales, Sydney, NSW, Australia.

### Retroviral constructs and viral transfection

Murine stem cell virus (MSCV)-based retroviral vectors carrying expression cassettes containing *HOXA9*, *MEIS1* and *MLL-AF9* have been described in our previous studies.<sup>1-3</sup> The retroviral MSCV-miR-101-puro, MSCV-miR-29b-puro and MSCV-miR-150-puro expression vectors were generated by GenScript (NJ, USA). pLX304-FOS-V5 was a gift from William Hahn (Addgene plasmid 59140)<sup>4</sup> and pLX304 was a gift from David Root (Addgene plasmid 25890).<sup>5</sup> Viral stocks were produced from 293T cells by transient transfection using Lipofectamine 2000. Virus-containing supernatants were harvested 48-72 hours post-transfection, filtered through 0.45- $\mu$ m membrane, and concentrated by centrifugation.

### Hematopoietic cell isolation, transduction and transplantation

HSPC-enriched LSK cells (Lin<sup>-</sup>CD127<sup>-</sup>Sca1<sup>+</sup>c-Kit<sup>+</sup>, BioLegend, Balcatta, WA, Australia) were flow-sorted from mouse BM as previously described.<sup>1,2,6</sup> To generate pre-LSCs, 3-5x10<sup>4</sup> HSPCs were incubated with concentrated virus carrying *MLL-AF9* or *HOXA9/MEIS1* supplemented with 7.5  $\mu$ g/ml polybrene (Sigma-Aldrich, Castle Hill, NSW, Australia). Two rounds of transduction were performed for each experiment. For mouse bone marrow transplantation, 1x10<sup>6</sup> GFP<sup>+</sup> pre-LSCs or 1x10<sup>5</sup> GFP<sup>+</sup> leukemic cells flow-sorted from primary AML mice were injected intravenously by the tail vein into sublethally irradiated (6 Gy) BL6 syngeneic recipient mice as previously described.<sup>1-3</sup>

### Fluorescence-activated cell sorting (FACS)

Alexa Fluor 647 anti-human CD45 antibodies were purchased from BioLegend (304018). Cells were stained with antibodies at 4 °C for 20 min before being subjected to FACS analysis using a BD LSRFortessa™ cell analyzer (BD Biosciences, North Ryde, NSW, Australia). Cell sorting was conducted using a BD Influx™ high-speed cell sorter (BD Biosciences). Flow cytometry data were analyzed using FlowJo software (TreeStar, Ashland, OR, USA).

### *In vitro* cell cycle and apoptosis

For cell cycle analysis, cells were fixed in ice-cold 70% ethanol for 2 hours at -20 °C, stained with anti-Ki67-Alexa Fluor 647 (BD Biosciences) and 7-amino-actinomycin D (7AAD, BD Biosciences) in staining solution (50  $\mu$ g/ml propidium iodide, 0.1% Triton X-100 and 100  $\mu$ g/ml DNase-free RNaseA) and incubated for 20 min at 4 °C prior to flow cytometric analysis. For apoptosis analysis, cells were incubated with Annexin V-APC staining solution (BD Biosciences, 550474) at room temperature for 10 minutes, followed by staining with 7-Aminoactinomycin D (7-AAD) (BD Biosciences, 559925) for 15 min on ice and subsequent analysis by flow cytometry.

### miRNA and mRNA gene expression profiling

Total mRNA was extracted using the RNeasy mini kit (Qiagen, Hilden, Germany, 74106) and miRNA was extracted using the miRNeasy mini kit (Qiagen, 217004). The array data are available in ArrayExpress under the accession numbers E-MTAB-7344, E-MTAB-7355 and E-MTAB-7356.

Labelling, hybridization and scanning were performed by the Ramaciotti Centre for Gene Function Analysis (University of New South Wales, Sydney, Australia), with mRNA hybridized to Illumina murine WG-6 v2.0 expression array for mRNA expression profiling and miRNA hybridized to Exiqon miRCURY LNA microRNA Array for global microRNA expression profiling. The mRNA expression profiling was analyzed using the GenePattern software (Broad Institute, MIT) as previously described.<sup>2</sup>

### **Bayesian Networks with Splitting-Averaging strategy used to identify miRNA-mRNA network**

A method called Bayesian network with splitting-averaging (BNSA) was used to identify complex miRNA-mRNA interactions for functional miRNA-mRNA regulatory networks (FMRMs). This method integrates miRNA-target information, sample-matched expression profiles of miRNA and mRNA, and sample categories. In order to capture all possible interactions, this method groups expression profiles of miRNAs and mRNAs together according to their sample category and then learns Bayesian Network (BN) structures on the relative expression changes of miRNA and mRNA in each category, respectively. The miRNA-target information acts as a constraint to guide the structure learning, whereby the miRNAs represent the parent nodes while the mRNAs are the descendant nodes. The edges linking the parent nodes to descendant nodes can only be those defined in the miRNA-target predictions. Interaction networks learned on each category are then integrated by BN averaging procedure. To avoid statistically insignificant results due to the small size of data sets, it uses bootstrapping to achieve reliable inference and integration.<sup>7</sup>

### **Cell viability assay**

Cell viability was measured by the AlamarBlue™ cell viability assay (Thermo Fisher Scientific, North Ryde, NSW, Australia, DAL1025) as per manufacturer's instruction. Briefly,  $5 \times 10^3$  human MOLM-13 cells were seeded in 96-well plates with 180  $\mu$ L media per well. After 48 hours 20  $\mu$ L of AlamarBlue reagent was added into each well and incubated at 37°C for 6 hours before absorbance values were measured at 570 and 595 nm using the Benchmark Plus microplate reader (Bio-Rad, Gladeville, NSW, Australia).

### **Colony formation assay**

Cells were seeded at a density of  $1 \times 10^3$  cells in 35 mm dishes in methylcellulose supplemented with mIL-3. Colonies were counted after 5 days incubation at 37°C. For serial replating assay, colonies were harvested, and  $1 \times 10^3$  cells were subsequently replated in fresh methylcellulose. Six rounds of serial replating were performed.

### **Real-time quantitative qPCR analysis (RT-qPCR) for gene expression**

Total RNA was extracted from cells using the RNeasy mini kit (Qiagen, 74106). cDNA was synthesized from total RNA using random primers (Thermo Fisher Scientific, 48190011) and M-MLV Reverse Transcriptase (Thermo Fisher Scientific, 28025013). RT-qPCR was performed using the Power SYBR® Green PCR Master Mix (Thermo Fisher Scientific, 436708) or SsoAdvanced Universal SYBR Green Supermix (Bio-Rad).

The values for target gene expression were normalized against the house-keeping gene Gapdh. RT-qPCR primers include mouse Bcl11a: forward 5'-GCGACACTTGTCCTTCACACACC-3', reverse 5'-GCTTCCATCCGAAAAGTCCACAC-3'; Mouse Meis2: forward 5'-GCAATCTATGGGCAC CCGTTGT-3', reverse 5'-CGGCGCGAACCTGCTTG-3'; mouse Six1: forward 5'-CAAGGAAAG

GGAGAACACCGA-3', reverse 5'-TGGAGCAGAAGGACCGAGT-3'; mouse Sall3 forward 5'-CACCCAAGCAGCACAACACTGTC-3', reverse 5'-TGCCCATGTGTACCTTGAGATTGC-3'; mouse Tcf7l2: forward 5'- TTCCTCCGATCACAGACCTGAG-3' and reverse: 5'-GCTGCCTTCA CCTTGTATGTAGC-3'; mouse p21: forward 5'-TTGCACTCTGGTGTCTGAGC-3' and reverse 5'- TGCGCTTGGAGTGATAGAAA-3'; mouse Gapdh: forward 5'-CTTTGTCAAGCTCATTTCC TGG-3' and reverse 5'-TCTTGCTCAGTGTCTTGC-3'.

### RT-qPCR analysis for miRNAs

miRNAs were extracted from cells using the miRNeasy mini kit (Qiagen, 217004). cDNA was synthesized using a Taqman microRNA reverse transcription (RT) kit (Life Technologies, Mulgrave, VIC, Australia, 4366596) and RT primers (Taqman microRNA assay 5X; Life Technologies, 4427975; see below for Assay details) specific for a target miRNA or a house-keeping miRNA. RT-qPCR was performed using the Taqman Universal PCR Mastermix II (2X), no UNG (Life Technologies, 4324018) and specific miRNA probes (Taqman microRNA assay 20X; see below for Assay details). The values for mouse and human miRNAs were normalized against their house-keeping genes, mouse snoRNA202 and human RNU48, respectively.

RT-qPCR primers for human and mouse miRNAs (Taqman)

	Assay Name	Assay ID
House-keeping miRNA for murine miRNAs	snoRNA202	001232
miR-101	mmu-miR-101	002507
miR-29a	mmu-miR-29a	002447
miR-29b	mmu-miR-29b	002497
miR-222	mmu-pri-miR-222	Mm03307187_pri
miR-150	mmu-miR-150	000473
House-keeping miRNA for human miRNAs	RNU48	001006
miR-101	hsa-miR-101	002253
miR-29a	hsa-miR-29a	002112
miR-29b	hsa-miR-29b	000413
miR-26b	hsa-miR-26b	000407
miR-27b	hsa-miR-27b	000409
miR-140	hsa-miR-140	002234
miR-222	hsa-miR-222	002276
miR-150	hsa-miR-150	000473

### Western blot analysis

Membranes were probed with antibodies against Meis1 (Abcam, Melbourne, VIC, Australia, ab124686), Mcl-1 (Abcam, ab32087), Bcl-2 (Genesearch, Arundel, QLD, Australia, 3498S), p21 (BD Biosciences, 556431), p27 (BD Biosciences, 610241), Gadd45a (Genesearch, 4632S), c-Fos (Genesearch, 4384S), phospho-c-Fos (Ser32; Genesearch, 5348S), Ezh2 (Genesearch, 3147S), H3K27me3 (Genesearch, 9733T), total H3 (Genesearch, 9715S), Actin (Sigma-Aldrich, A2066) and GAPDH (Abcam, ab8245). Densitometry was performed using NIH ImageJ software. Protein band intensity was normalized against loading control (Actin, GAPDH or H3) and compared to relative control.

### **Confocal immunofluorescence**

4 x 10<sup>4</sup> cells were cytospun onto glass slides, fixed in 4% paraformaldehyde in PBS for 10 minutes at room temperature and then washed three times for 5 minutes in PBS with 0.1% Tween-20 (PBS-T). Non-specific antibody binding was blocked with blocking media (10% goat serum and 2% BSA in PBS-T) for 1 hour. Slides were stained overnight at 4C with a mouse monoclonal antibody against non-phospho (active)  $\beta$ -catenin (Ser33/Ser37/Thr41; clone 8E7, Merck, Bayswater, VIC, Australia, 05-665) at a dilution of 1:100, washed three times for 5 minutes in PBS-T, and then stained for 1 hour with Alexa Fluor 568-conjugated donkey anti-mouse secondary antibody (Abcam, ab175472) at a dilution of 1:500 and washed three times with PBS-T for 5 minutes followed by staining with DAPI (1:4000, Thermo Fisher Scientific) for 30 minutes. Coverslips were mounted with ProLong Gold antifade mountant (Thermo Fisher Scientific) and edges were sealed with nail polish to prevent desiccation. Immunofluorescence images were taken with a TCS SP5 MP-STED confocal microscope (Leica Microsystems, Mannheim, Germany) and processed using NIH ImageJ software.

### ***In vivo* bioluminescence imaging of NSG mice**

GFP-luciferase-expressing human MOLM-13 AML cells were generated by transducing retroviral vector SFG-NES-TGL (GFP-FLuc; a gift from Vladimir Ponomarev)<sup>8</sup> into MOLM-13 cells (ATCC, Noble Park North, VIC, Australia; recently authenticated by Short Tandem Repeat PCR and tested for mycoplasma contamination) followed by flow-sorting of GFP<sup>+</sup> transduced cells. 5 x 10<sup>5</sup> transduced cells were injected intravenously by the tail vein into NSG mice, which were monitored for assessing *in vivo* engraftment of human AML cells using non-invasive bioluminescent imaging. Images were taken 10 min after intraperitoneal injection of D-luciferin (150 mg/kg of body weight; Promega, P1043) for FLuc signals detected by the IVIS Spectrum CT (Caliper Life Sciences, MA, USA).<sup>8,9</sup> Signal intensity quantification and analysis were performed using the Living Image 4.5.5 software (Perkin Elmer, Waltham, MA, USA). The bioluminescent signal was recorded as radiance photons/sec/cm<sup>2</sup>/steradian (p/s/cm<sup>2</sup>), represented in pseudocolor to indicate the signal intensities.

### **Luciferase Reporter Assay**

For transfection, 6x10<sup>3</sup> 293T cells/well were plated in 96-well plates in triplicate for each condition. After incubation overnight, cells were transfected with 20 ng of the pMIR-REPORT plasmid (pMIR-REPORT miRNA expression vector system; Thermo Fisher Scientific, AM5795) bearing the 3'UTR of *c-FOS*, and 20 ng of MSCV-miR-101-puro or MSCV-miR-150-puro versus control empty vector (EV) using Lipofectamine 3000 (Thermo Fisher Scientific, L3000015). pMIR-REPORT<sup>TM</sup> Beta-galactosidase Reporter Control Vector (Thermo Fisher Scientific, AM5795) (1 ng) was cotransfected for transfection efficiency control in all transfections. Transduced cells were lysed, and firefly luciferase and  $\beta$ -galactosidase activities were detected using Dual-Light<sup>®</sup> Luciferase &  $\beta$ -Galactosidase Reporter Gene Assay System (Thermo Fisher Scientific, T1003/T1004) 48h post-transfection following the manufacturer's protocol. Firefly luciferase activity was normalized to  $\beta$ -galactosidase activity for each transfected well. Each experiment was performed in triplicate and repeated three times.

### **Statistical analysis**

Statistical significance of differences was determined by an unpaired two-tailed Student's *t*-test for comparison between two groups and log-rank test for Kaplan-Meier survival curves using GraphPad Prism 7 (La Jolla, CA, USA). Data are presented as mean  $\pm$  SEM. \**P* < 0.05, \*\**P* < 0.005, \*\*\**P* < 0.0005, \*\*\*\**P* < 0.0001, *NS* = Not Significant.

## References

1. Krivtsov AV, Twomey D, Feng Z, Stubbs MC, Wang Y, Faber J, et al. Transformation from committed progenitor to leukaemia stem cell initiated by MLL-AF9. *Nature*. 2006;442(7104):818-822.
2. Wang Y, Krivtsov AV, Sinha AU, North TE, Goessling W, Feng Z, et al. The Wnt/beta-catenin pathway is required for the development of leukemia stem cells in AML. *Science*. 2010;327(5973):1650-1653.
3. Dietrich PA, Yang C, Leung HH, Lynch JR, Gonzales E, Liu B, et al. GPR84 sustains aberrant beta-catenin signaling in leukemic stem cells for maintenance of MLL leukemogenesis. *Blood*. 2014;124(22):3284-3294.
4. Shao DD, Xue W, Krall EB, Bhutkar A, Piccioni F, Wang X, et al. KRAS and YAP1 converge to regulate EMT and tumor survival. *Cell*. 2014;158(1):171-184.
5. Yang X, Boehm JS, Yang X, Salehi-Ashtiani K, Hao T, Shen Y, et al. A public genome-scale lentiviral expression library of human ORFs. *Nat Methods*. 2011;8(8):659-661.
6. Osawa M, Hanada K, Hamada H, Nakauchi H. Long-term lymphohematopoietic reconstitution by a single CD34-low/negative hematopoietic stem cell. *Science*. 1996;273(5272):242-245.
7. Liu B, Li J, Tsykin A, Liu L, Gaur AB, Goodall GJ. Exploring complex miRNA-mRNA interactions with Bayesian networks by splitting-averaging strategy. *BMC Bioinformatics*. 2009;10:408.
8. Ponomarev V, Doubrovin M, Serganova I, Vider J, Shavrin A, Beresten T, et al. A novel triple-modality reporter gene for whole-body fluorescent, bioluminescent, and nuclear noninvasive imaging. *Eur J Nucl Med Mol Imaging*. 2004;31(5):740-751.
9. Schaub FX, Reza MS, Flavény CA, Li W, Musicant AM, Hoxha S, et al. Fluorophore-NanoLuc BRET Reporters Enable Sensitive In Vivo Optical Imaging and Flow Cytometry for Monitoring Tumorigenesis. *Cancer Res*. 2015;75(23):5023-5033.